Supplementary Information (SI) for Nanoscale.

Supplementary Information

Phase-engineered 1T′/2H-MoS_2 heterophase junctions for high-performance aqueous zinc-ion batteries

Xue-Wei Lu, Xuetao Li, Ruxuan Chen, Shuwei Wang, Zile Wang and Cong Chao*

Key Laboratory of Power Station Energy Transfer Conversion and System of Ministry of Education and School of Energy Power and Mechanical Engineering, and Beijing Laboratory of New Energy Storage Technology, North China Electric Power University, Beijing, 102206, China.

Corresponding Author:
E-mail address: 50202891@ncepu.edu.cn

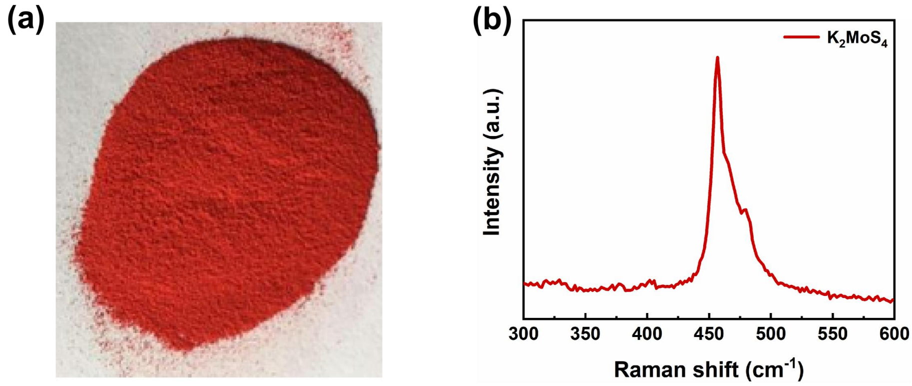

Figure S1. (a) Photograph of the K_2MoS_4 precursor and (b) its corresponding Raman spectrum.

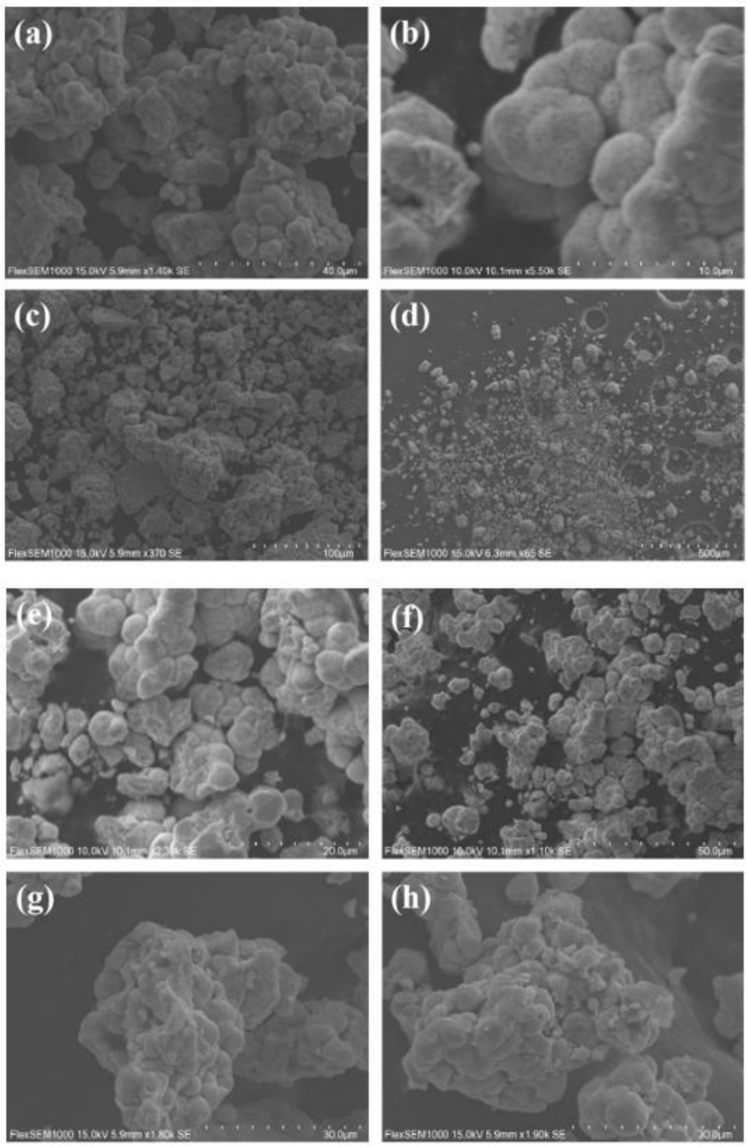

Figure S2. SEM images of MoS_2 samples synthesized via hydrothermal method under varying conditions: (a) 200 °C for 12 h, (b) 180 °C for 12 h, and (c) 200 °C for 24 h.

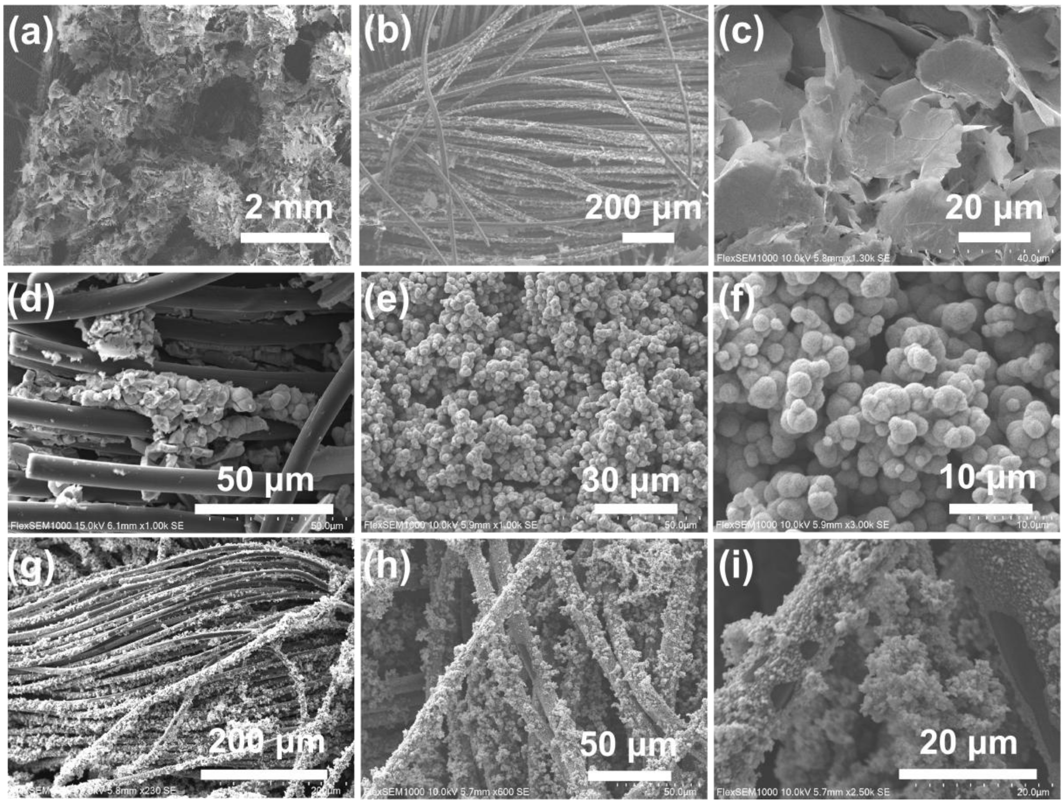

Figure S3. SEM images of MoS_2 samples grown on carbon cloth using different precursors: (a–c) K_2MoS_4, (d–f) $Na_2MoO_4{\cdot}2H_2O$ with thiourea, and (g–i) $(NH_4)_2MoO_4$ with thiourea.

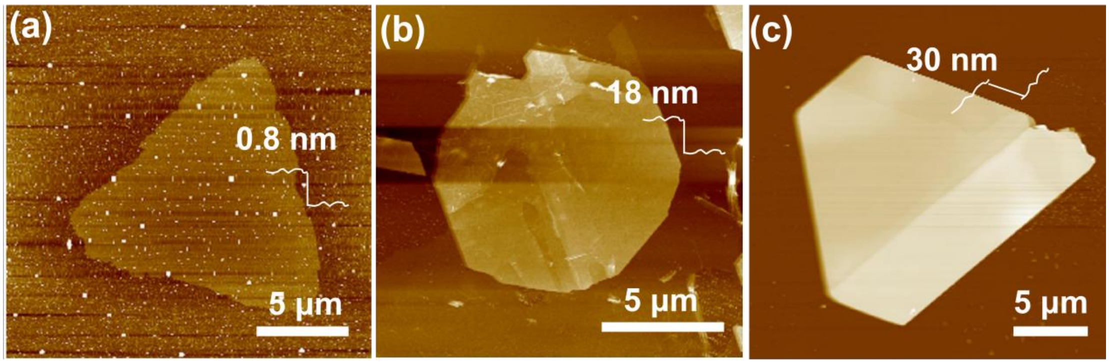

Figure S4. Atomic force microscopy (AFM) images of 1T′/2H-MoS_2 with varying thicknesses: (a) 0.8 nm (monolayer), (b) 18 nm, and (c) 30 nm.

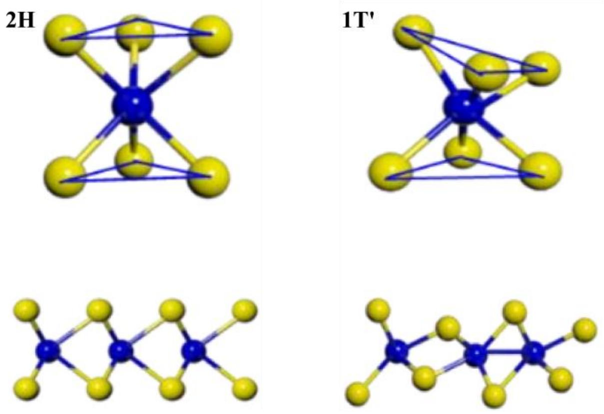

Figure S5. Atomic structure schematics comparing the hexagonal (2H-phase, left) and distorted octahedral (1T′-phase, right) configurations of MoS_2.

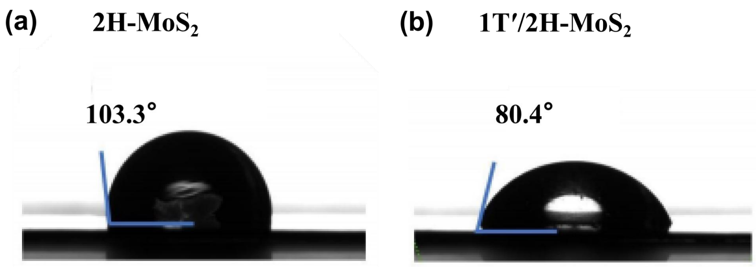

Figure S6. Water contact angles of (a) 2H-MoS_2 and (b) 1T′/2H-MoS_2.

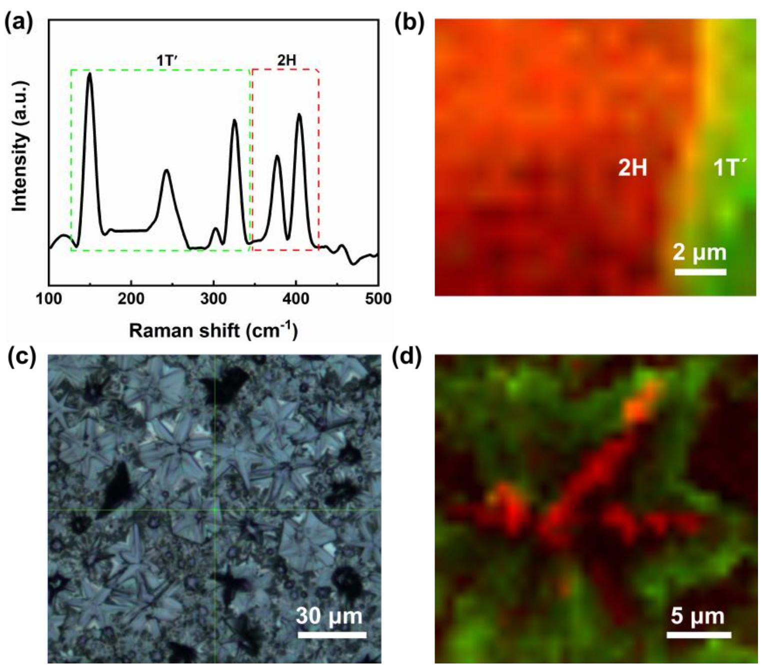

Figure S7. (a) Raman spectrum and (b) Raman area mapping of 1T′/2H-MoS_2. (c) Optical micrograph of hexagonal star-shaped 1T′/2H-MoS_2 crystals grown on mica substrates by controlled thermal evaporation, with (d) corresponding Raman area mapping.

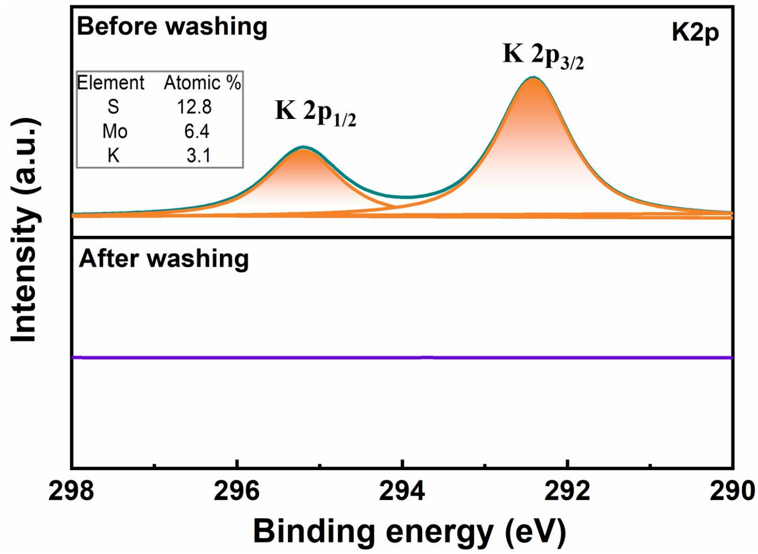

Figure S8. XPS spectra of the K 2p orbital in 1T′/2H-MoS_2 before (top) and after (bottom) aqueous washing treatment.

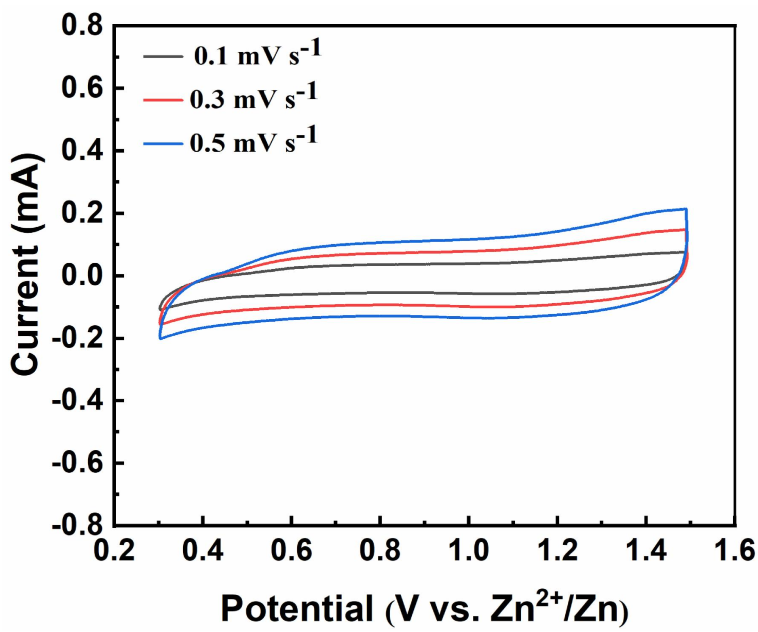

Figure S9. Cyclic voltammetry (CV) profiles of 2H-MoS_2 at various scan rates.

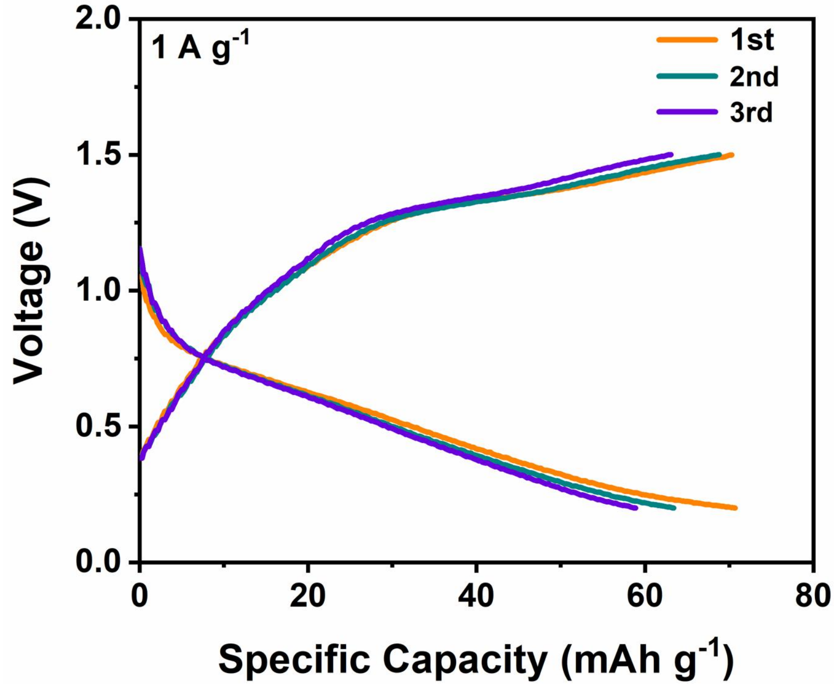

Figure S10. Galvanostatic charge-discharge profiles of 2H-MoS_2 cathode at a current density of 1 A g^{-1}.

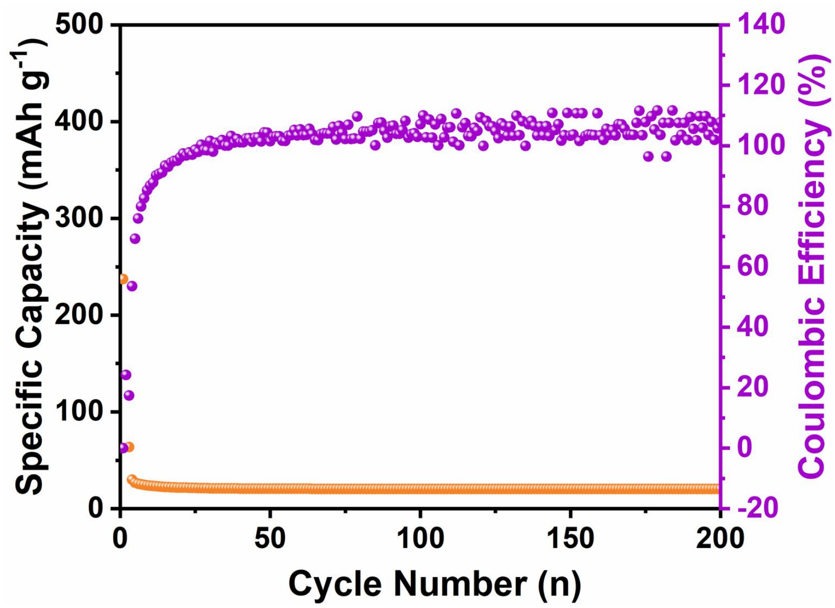

Figure S11. Long-term cycling stability of 2H-MoS_2 cathode at a current density of 1 A g^{-1}.

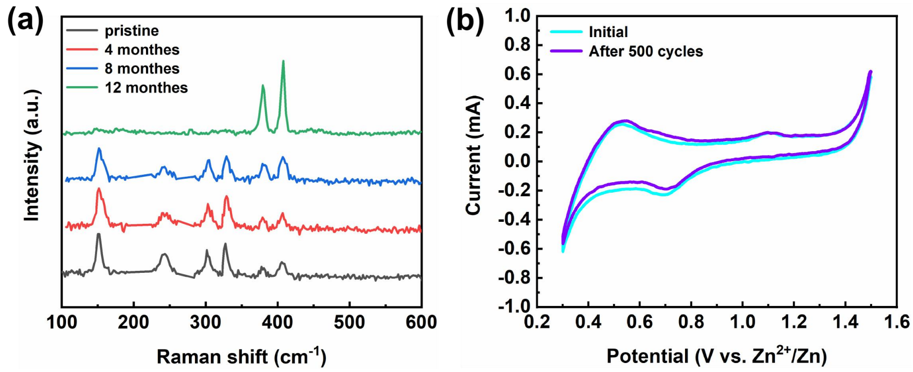

Figure S12. Stability evaluation measurements of 1T′/2H-MoS_2.

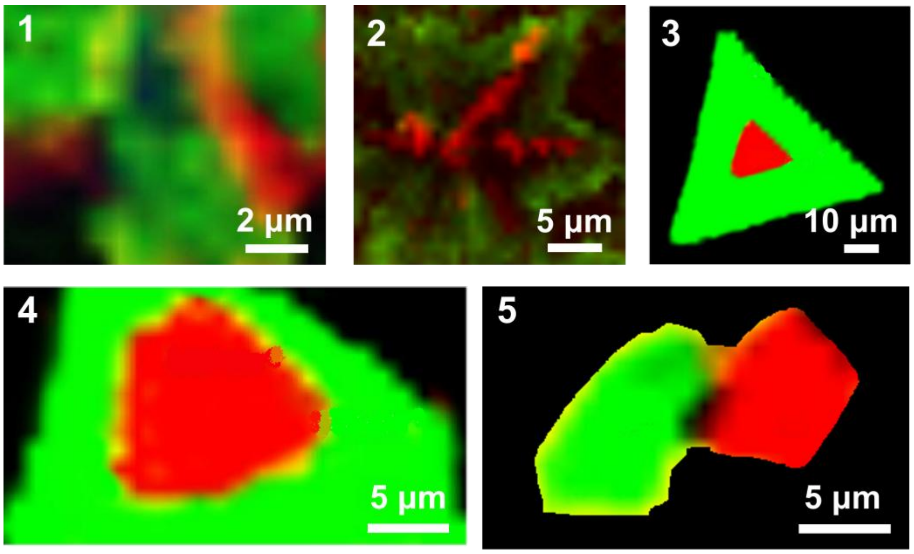

Figure S13. Raman mapping analysis of the spatial distribution and phase composition. The green and red regions represent the 1T′ and 2H domains, respectively.

Table S1 The ICP-OES result of 1T′/2H-MoS_2.

Content	K (wt.%)	Mo (wt.%)	S (wt.%)
1T′/2H-MoS_2	0	62.663	37.337

Table S2 Area statistics of 1T′ and 2H domains based on Raman mapping.

Sample number	Area percent of 1T′ phase	Area percent of 2H phase
1	69.2%	30.8%
2	62.3%	37.7%
3	89.8%	10.2%
4	81.5%	18.5%
5	58.8%	41.2%

Table S3 Comparison of the Zn-ion storage performance of 1T′/2H-MoS_2 cathode in this work with those of recently reported cathodes for aqueous zinc-based batteries.

Cathode	Electrolyte	Voltage (V)	Capacity at 1 A g^{-1} (mAh g^{-1})	Cycle Stability	Ref.
1T′/2H-MoS_2	**2M $ZnSO_4$**	**0.3-1.5**	**150**	86.4% after 2000 cycles at 1 A g^{-1} 69.5% after 4000 cycles at 1 A g^{-1}	**This work**
MoS_2-O	3M $Zn(CF_3SO_3)_2$	0.2-1.4	95	68% after 2000 cycles at 1.0 A g^{-1}	[1]
MoS2-160	3M $Zn(CF_3SO_3)_2$	0.2-1.2	126	98.1% after 400 cycles at 1.0 A g^{-1}	[2]
MoS_{2-x}	3M $Zn(CF_3SO_3)_2$	0.2-1.2	95.6	87.8% after 1000 cycles at 1.0 A g^{-1}	[3]
MoS_2/PANI	3M $Zn(CF_3SO_3)_2$	0.2-1.3	106.1	86% after 1000 cycles at 1.0 A g^{-1}	[4]
VS_2@VOOH	3M $Zn(CF_3SO_3)_2$	0.4-1.0	124	86% after 200 cycles at 0.5 A g^{-1}	[5]
MoS_2@CNTs	3M $Zn(CF_3SO_3)_2$	0.3-1.2	112.8	80.1% after 500 cycles at 1.0 A g^{-1}	[6]
WS_2-200	1M $ZnSO_4$	0.1-1.5	85.11	0% after 100 cycles at 0.2 A g^{-1}	[7]
VSe_2	2M $ZnSO_4$	0.1-1.6	93.9	80.8% after 500 cycles at 0.1 A g^{-1}	[8]
TiS_2	2M $ZnSO_4$	0.05-1.0	76	70% after 500 cycles at 1 A g^{-1}	[9]
MnO_2@N	2 M $ZnSO_4$ + 0.5 M $MnSO_4$	1.0-1.8	125	83% after 1000 cycles at 5 A g^{-1}	[10]
Ti-MnO_2	3M $Zn(CF_3SO_3)_2$ + 0.1M $Mn(CF_3SO_3)_2$	0.8-1.8	175	86.9% after 200 cycles at 0.1 A g^{-1}	[11]
Mn-d-ZMO@C	2 M $ZnSO_4$ + 0.2 M $MnSO_4$	0.8-1.9	170	84% after 2000 cycles at 3.0 A g^{-1}	[12]
DHPBA-Fe (II)	1M $ZnSO_4$	0.25-2.25	92.5	99.2% after 1000 cycles at 2.0 A g^{-1}	[13]
COF-TMT-BT	2M $Zn(CF_3SO_3)_2$	0.5-1.6	180	65.9% after 2000 cycles at 0.1 A g^{-1}	[14]
DDA-Cu	3.5M $Zn(CF_3SO_3)_2$	0.2-1.6	150	99% after 100 cycles at 2.0 A g^{-1}	[15]

References

1 H. Liang, Z. Cao, F. Ming, W. Zhang, D. H. Anjum, Y. Cui, L. Cavallo and H. N. Alshareef, Aqueous Zinc-Ion Storage in MoS_2 by Tuning the Intercalation Energy, *Nano Lett.*, 2019, **19** (5), 3199-3206.

2 J. Liu, P. Xu, J. Liang, H. Liu, W. Peng, Y. Li, F. Zhang and X. Fan, Boosting aqueous zinc-ion storage in MoS_2 via controllable phase, *Chem. Eng. J.*, 2020, **389**, 124405.

3 W. Xu, C. Sun, K. Zhao, X. Cheng, S. Rawal, Y. Xu and Y. Wang, Defect engineering activating (Boosting) zinc storage capacity of MoS_2, *Energy Storage Mater.*, 2019, **16**, 527-534.

4 M. Huang, Y. Mai, L. Zhao, X. Liang, Z. Fang and X. Jie, Tuning the kinetics of zinc ion in MoS2 by polyaniline intercalation, *Electrochim. Acta*, 2021, **388**, 138624.

5 X. Pu, T. Song, L. Tang, Y. Tao, T. Cao, Q. Xu, H. Liu, Y. Wang and Y. Xia, Rose-like vanadium disulfide coated by hydrophilic hydroxyvanadium oxide with improved electrochemical performance as cathode material for aqueous zinc-ion batteries, *J. Power Sources*, 2019, **437**, 226917.

6 M. Huang, Y. Mai, L. Zhao, X. Liang, Z. Fang and X. Jie, Hierarchical MoS_2@CNTs Hybrid as a Long-Life and High-Rate Cathode for Aqueous Rechargeable Zn-Ion Batteries, *ChemElectroChem*, 2020, **7** (20), 4218-4223.

7 B. Tang, N. Tian, J. Jiang, Y. Li, J. Yang and Q. Zhu, Investigation of zinc storage capacity of WS_2 nanosheets for rechargeable aqueous Zn-ion batteries, *J. Alloys Compd.*, 2022, **894**, 162391.

8 Z. Wu, C. Lu, Y. Wang, L. Zhang, L. Jiang, W. Tian, C. Cai, Q. Gu, Z. Sun and L. Hu, Ultrathin VSe2 Nanosheets with Fast Ion Diffusion and Robust Structural Stability for Rechargeable Zinc-Ion Battery Cathode, *Small*, 2020, **16** (35), 2000698.

9 L. Wang, M. Jiang, F. Liu, Q. Huang, L. Liu, L. Fu and Y. Wu, Layered TiS_2 as a Promising Host Material for Aqueous Rechargeable Zn Ion Battery, *Energy Fuels*, 2020, **34** (9), 11590-11596.

10 Y. Zhang, Y. Liu, Z. Liu, X. Wu, Y. Wen, H. Chen, X. Ni, G. Liu, J. Huang and S. Peng, MnO_2 cathode materials with the improved stability via nitrogen doping for aqueous zinc-ion batteries, *J. Energy Chem.*, 2022, **64**, 23-32.

11 S. Lian, C. Sun, W. Xu, W. Huo, Y. Luo, K. Zhao, G. Yao, W. Xu, Y. Zhang, Z. Li, K. Yu, H. Zhao, H. Cheng, J. Zhang and L. Mai, Built-in oriented electric field facilitating durable Zn MnO_2 battery, *Nano Energy*, 2019, **62**, 79-84.

12 S. Islam, M. H. Alfaruqi, D. Y. Putro, S. Park, S. Kim, S. Lee, M. S. Ahmed, V. Mathew, Y. K. Sun, J. Y. Hwang and J. Kim, In Situ Oriented Mn Deficient $ZnMn_2O_4$@C Nanoarchitecture for Durable Rechargeable Aqueous Zinc-Ion Batteries, *Adv. Sci.*, 2021, **8** (4), 2002636.

13 W. D. Zhang, Y. Zou, H. Zhao, M. Chen, L. Zhou, X. R. Xie, X. Yan, H. Pang and Z. G. Gu, Double-Shelled Open Hollow Metal-Organic Frameworks for Efficient Aqueous Zn-Ion Batteries, *Small*, 2023, **20**, 2307809.

14 H. Peng, S. Huang, V. Montes-García, D. Pakulski, H. Guo, F. Richard, X. Zhuang, P. Samorì and A. Ciesielski, Supramolecular Engineering of Cathode Materials for Aqueous Zinc-ion Energy Storage Devices: Novel Benzothiadiazole Functionalized Two-Dimensional Olefin-Linked COFs, *Angew. Chem. Int. Ed.*, 2023, **62**, e202216136.

15 C. Yang, K. Feng, J. Chen, Z. Liu and Y. Yu, A Cu-based electronically conducting metal–organic framework with π–d conjugation for cathode and anode modification in aqueous zinc-ion batteries, *Chem. Eng. J.*, 2025, **520**, 165857.